PROCEEDINGS OF THE ROYAL SOCIETY A MATHEMATICAL, PHYSICAL & ENGINEERING SCIENCES

The circular hydraulic jump in low gravity

C. T. Avedisian and Z. Zhao

Proc. R. Soc. Lond. A 2000 **456**, doi: 10.1098/rspa.2000.0606, published 8 September 2000

10.1098/rspa.2000.0606

THE ROYAL SOCIETY

The circular hydraulic jump in low gravity

By C. T. Avedisian and Z. Zhao†

Sibley School of Mechanical and Aerospace Engineering, Cornell University, Ithaca, NY 14853-7501, USA

Received 9 September 1999; accepted 5 January 2000

An experimental study of the circular hydraulic jump (CHJ) was carried out to show how reducing gravity to 10^{-2} times that of the Earth's normal gravity affects the CHJ diameter and the downstream flow patterns. Water was the working fluid. Measurements of the CHJ diameter and the shape of the free liquid surface across the jump were made in low gravity using the downstream fluid height and the flow rate as the parameters. Comparisons are made with normal-gravity flow conditions. A drop tower was used to create low gravity. The measurements are compared with an existing theory for predicting how gravity affects the CHJ diameter.

Results show that the steady-state CHJ diameter is larger at low gravity than normal gravity. As the downstream fluid height is increased, the CHJ diameter at normal gravity moves inward, but at low gravity the CHJ diameter does not show a similar influence of downstream fluid height. The curvature across the CHJ is higher at normal gravity than at low gravity and the length of the transition zone from the upstream to downstream height increases as gravity is reduced. Waves in the downstream flow are observed for all low-gravity flow conditions but at normal gravity they were observed only for selected flow conditions, suggesting that the influence of surface tension and viscosity dominate at low gravity. Measured normal-gravity and low-gravity CHJ diameters were bounded by theoretical predictions which assume either fully developed or developing flow conditions for the upstream thin film.

Keywords: hydraulic jump; jet impingement; low gravity; waves; liquid film; impingement cooling

1. Introduction

Impingement of a circular liquid jet onto a solid surface is important in a variety of cooling processes: impingement cooling of electronic devices, materials processing in manufacturing, laser mirrors, aircraft generator coils and vapour absorption refrigeration cycles. A feature of impinging liquid jets is their potential for dissipating high heat transfer rates because of the small liquid film thickness and high flow velocity. For example, the highest steady-state heat fluxes reported in any configuration were achieved by a water jet impinging onto a plasma heated surface (Liu & Lienhard 1993*a*).

General features of a liquid jet impinging onto a solid surface are shown in figure 1. During radial spread away from the stagnation point, a circular hydraulic jump (CHJ) may form. The lower flow velocity downstream of the CHJ relative to

† Present address: Broadcom Corp., 2099 Gateway Place, Suite 700, San Jose, CA 95110, USA.

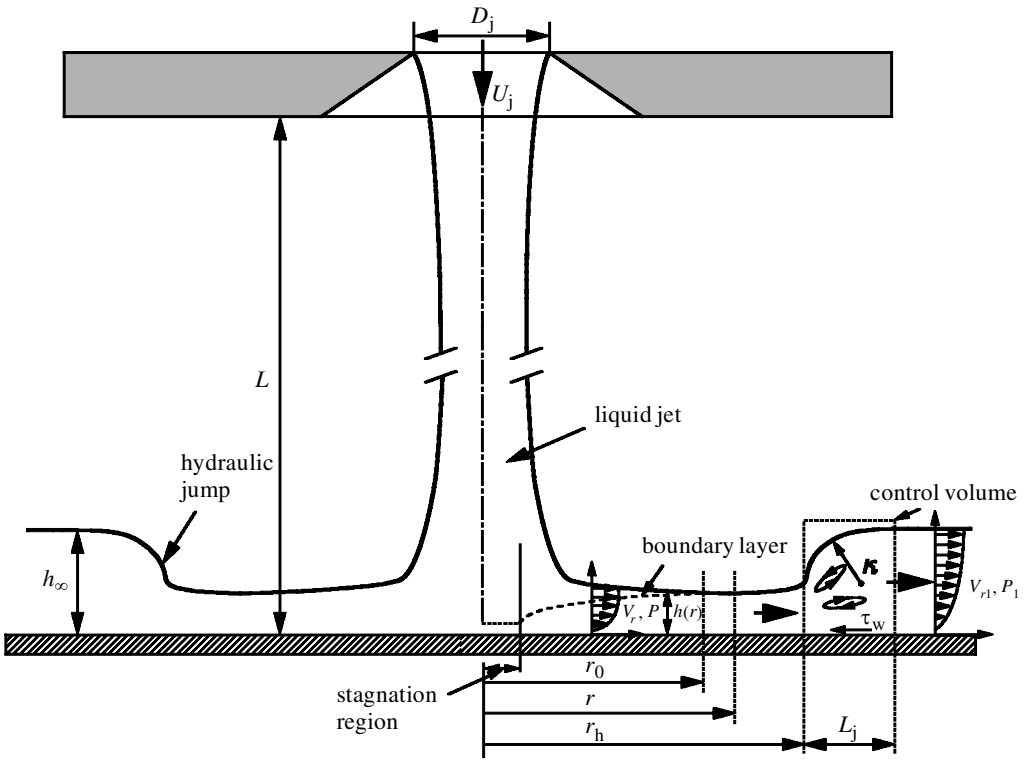

Figure 1. Schematic of jet impingement structure.

the upstream velocity in the thin film motivates predicting the parameters upon which the CHJ depends because of the potential for reduced heat transfer in the downstream flow in applications where a cold impinging jet is used to cool a hot target plate (see, for example, Womac *et al*. 1993).

In this paper we present new data and observations which show the influence of lowering gravity on the CHJ. The parameters are the liquid height downstream of the CHJ, the volumetric flow rate and the jet orifice opening. The magnitude of 'low' gravity employed in the present study is nominally 0.02 that of Earth's normal gravity, which is achieved by carrying out the experiments in a laboratory frame that is literally dropped or in freefall. Specific objectives were the following: (1) obtain photographic documentation to show how a CHJ is affected by reducing gravity; (2) measure the CHJ diameter and shape of the liquid surface in the transition zone in low gravity and compare the results with normal-gravity observations; and (3) compare the measurements with prior analysis of jet impingement as applied to low gravity.

Gravity affects the location of the CHJ, the curvature of free surface across the jump and the length of the transition zone across the jump (L_j in figure 1). These effects are most directly shown by considering the case of an inviscid fluid (§ 2 reviews some prior analyses of a CHJ) and a CHJ that is a discontinuity in the flow ($L_j = 0$). Middleman (1995) provides details and only a brief summary is given here. A momentum balance on a control volume (see figure 1) across a CHJ relates the change in momentum of the fluid to the change of the force of the pressure due to the differing

film thicknesses upstream and downstream of the jump (see the Nomenclature for a definition of symbols):

$$\int_0^{h_\infty} V_{r1}^2\,\mathrm{d}z - \int_0^{h} V_r^2\,\mathrm{d}z = \int_0^{h} P\,\mathrm{d}z - \int_0^{h_\infty} P_1\,\mathrm{d}z. \tag{1.1}$$

Since we are considering a frictionless fluid (analyses which include viscosity are discussed in § 4 *c*), equation (1.1) can be integrated directly because V_r and V_{r1} are independent of z for the frictionless case. Combining the result with mass conservation gives

$$\left(\frac{r_j^2 U_j}{2r_h}\right)^2 \left(\frac{1}{h} - \frac{1}{h_\infty}\right) = \tfrac{1}{2} G g_0 (h_\infty^2 - h^2), \tag{1.2}$$

where $G = g/g_0$. A well-known relationship between the ratio of downstream to upstream film thickness follows by expressing equation (1.2) in non-dimensional form:

$$H_\infty/H = \tfrac{1}{2}\{\sqrt{1 + 8Fr} - 1\}, \tag{1.3}$$

where the Froude number (Fr) based on the average velocity (U) of the liquid film just upstream of the jump is U^2/Gg_0h and mass conservation was used to relate U_j to U. A relationship between the CHJ diameter and flow parameters follows from equation (1.2) by substituting for h the expression obtained from a mechanical energy balance applied across the CHJ (i.e. $h = r_j^2/2r_h$),

$$D_h = \frac{1}{H_\infty}(Fr_j - \tfrac{1}{2}), \tag{1.4}$$

where Fr_j denotes the grouping of terms U_j^2/Gg_0h_∞ and, from mass conservation, $Fr_j = Fr(4D_h^2H^3/H_\infty)$. Equation (1.4) shows the influence of gravity on D_h for the inviscid model for given h_∞; $D_h \propto 1/G$. When $G = 0$, D_h should be infinite (which means that a CHJ will not form and the flow is 'supercritical' throughout in the sense that $Fr \gg 1$ everywhere). More practical is that if $0 < G < 1$, D_h should be larger in low gravity than normal gravity.

Gravity also affects the free surface radius, κ (see figure 1), across the transition zone of the jump. To consider these influences, the assumption of the CHJ as a discontinuity has to be relaxed. In general terms the radius of curvature of the free surface in the transition zone across the CHJ is determined by balancing the hydrostatic pressure in the downstream film with the surface tension force at the liquid–air interface. In non-dimensional form,

$$\bar{\kappa} \approx 1/Bo, \tag{1.5}$$

where the Bond number is defined as $Bo \equiv \rho G g_0 h_\infty r_j/2\sigma$ and $\bar{\kappa} \equiv \kappa/r_j$. From equation (1.5), $\bar{\kappa} \propto 1/G$, whereby decreasing G increases the radius of curvature, and the transition to the downstream flow should be more gradual in low gravity compared with $G = 1$. Associated with the increase of $\bar{\kappa}$ as G is lowered is a lengthening of the transition region across the jump (L_j in figure 1). For *planar* hydraulic jumps, Hager (1993) shows experimentally that L_j is related to Fr as

$$L_j = C_1 + C_2 \tanh(C_3\sqrt{Fr}), \tag{1.6}$$

where the hyperbolic tangent form was found to best represent the measurements, which also determine the constants. Equations (1.5) and (1.6) together show that reducing gravity should make the transition across the jump more gradual.

From the above equations, two non-dimensional groups affect the CHJ when viscosity is negligible: the Froude number and the Bond number. The Reynolds number enters when viscous effects are important. Parameters upon which these non-dimensional groups depend can be adjusted in many ways to give the same dynamic effect, and except for G they have all been investigated in past work. For example, increasing the upstream velocity produces the same effect on the CHJ position as decreasing the downstream film height; increasing the radius of curvature across the jump can be accomplished by increasing the fluid surface tension or lowering the downstream film height, and so forth. As will be shown, several unique effects arise by lowering gravity that are not readily explainable by existing theories.

2. Brief review of prior work

An extensive literature exists on jet impingement in general and the hydraulic jump in particular. Standard fluid mechanics textbooks provide basic formulations for planar inviscid hydraulic jumps (see, for example, Allen & Ditsworth 1972; Streeter *et al.* 1998). Examples of recent studies that extend these treatments include work by Hornung *et al.* (1995), who include vorticity generation in the downstream flow of a planar jump, and Higuera (1994), who developed a model for a planar jump including flow in the transition region taking into account surface tension for the limit of infinite Reynolds number.

Nirapathdongporn (1968) reviews the literature on the CHJ prior to 1968, and Middleman (1995) provides an excellent pedagogical review of CHJ analyses. One of the earliest theories of a CHJ was by Tani (1949) (with the basic analysis later included in the study by Bouhadef (1978)), who analysed boundary layer flow of a viscous fluid and identified flow conditions where $\mathrm{d}h/\mathrm{d}r$ (figure 1) is infinite. Before reaching this condition Tani (1949) speculates that the flow separates and displaces the film upward. Errico (1986) also reviews some of the theories for the CHJ and presents measurements at $G = 1$ that show various levels of agreement with analyses. Watson (1964) derives a self-similar solution to the boundary layer equations upstream of the jump, assumes inviscid flow downstream of the jump and applies the momentum balance (equation (1.1)) to derive an expression for the CHJ diameter for the limit of infinite Froude number. Bowles & Smith (1992) extend Watson's analysis to include surface tension, the formation of small standing waves upstream of the jump and the cross-stream pressure gradient due to streamline curvature. The numerical solution by Chaudhury (1964) accounts for the effect of turbulence and heat transfer and predicts both the CHJ diameter and film thickness downstream of the jump. Experiments reported by Craik *et al.* (1981) are noteworthy for the insights they provided on the flow structure within and behind a CHJ. Back-flow, separation and eddies were observed near the CHJ. The role of surface tension on stabilizing a CHJ and promoting separation of the flow at $G = 1$ was examined in experiments by Liu & Lienhard (1993*b*).

The effect of gravity has not specifically been addressed in prior experiments on the CHJ. The closest one comes is the experimental study of Labus (1976) on jet impingement flows at $G \ll 1$ carried out in a drop tower. The focus was on studying

the shapes assumed by a free liquid surface rolling off of the edge of a pedestal on which a liquid jet impinged in a $G \ll 1$ environment. Labus (1976) noted that no CHJ occurred during any of the $G \ll 1$ tests but that they were a common occurrence at $G = 1$ for nominally the same upstream flow conditions. Reducing gravity thus appeared to push the CHJ off the target plate for the flow conditions examined. Concerning analysis, a number of numerical and analytical studies specifically referenced the condition $G = 0$. Simplified one-dimensional analysis of jet impingement flows (Thomas *et al.* 1990) and direct numerical simulations (Rahman *et al.* 1990) predict that the CHJ diameter is infinite, or equivalently that a CHJ does not form, when $G = 0$, which is consistent with equation (1.4).

3. Experimental design

A low-gravity environment for the present experiments was created by using a drop tower in which the flow loop and associated instrumentation are dropped. Low gravity is created in the moving frame of reference during the package's downward flight. Because we had a limited period of free-fall, the simplest way to examine gravity's effect on the jet impingement flow structure and the CHJ diameter was to first establish a CHJ at $G = 1$ then, with cameras in operation, rapidly reduce gravity. In this way we could observe the transient nature of the adjustment of the CHJ to the change in gravity as well as the steady-state structure of the CHJ in the low-G environment. The package containing the flow loop was released into free-fall by deactivating a magnet which initially held the package to the support ceiling. The general drop tower facility was described previously (Avedisian *et al.* 1988). It provides free-fall over a 7.6 m distance of an instrumentation package which houses the experiment to give an experimental run time of about 1.25 s.

The gravity level in the moving frame of reference increases from zero immediately upon release of the package because of air drag. Measurements of G within the falling package used in this study showed G reaching 0.05 after 1.2 s. An average value for the 1.2 s duration of the free fall is 0.02 and this is the value which we mean by the terms 'low gravity' and '$G \ll 1$'.

A schematic of the flow loop is shown in figure 2. The components are the following: recirculating pump; plenum containing beads, a flow straightener (to dampen the inlet flow) and a removable orifice plate attached at one end; Plexiglas chamber within which the target plate is mounted; flow control valve; and cameras and lighting. The height of the liquid level downstream of the jump is controlled by partly submerging the target plate and raising the water level to the desired height above the plate. The experimental conditions examined were the following. The downstream fluid height, h_∞, was 2.0, 4.0, 6.0, 10.0 or 15.0 mm. The liquid flow rates varied between 2.39 and 26.5 ml s^{-1}. To create laminar jets, a sharp-edged orifice was used. Orifice diameters of 1.22, 2.56 and 3.83 mm were used. They were machined into a stainless steel plate that was bolted to the bottom of the plenum. Figure 3 shows the design. The plenum chamber (figure 4) was mounted such that the orifice was 7.62 cm above the target surface.

The target plate was a 6.35 mm thick and 23 cm diameter Pyrex glass disc. The glass disc was in turn attached to a Plexiglas support disc 1.9 cm thick and 23 cm in diameter and mounted to one end of a circular Plexiglas cylinder that was then bolted to the containment vessel and sealed with o-rings. A mirror tilted to 45°

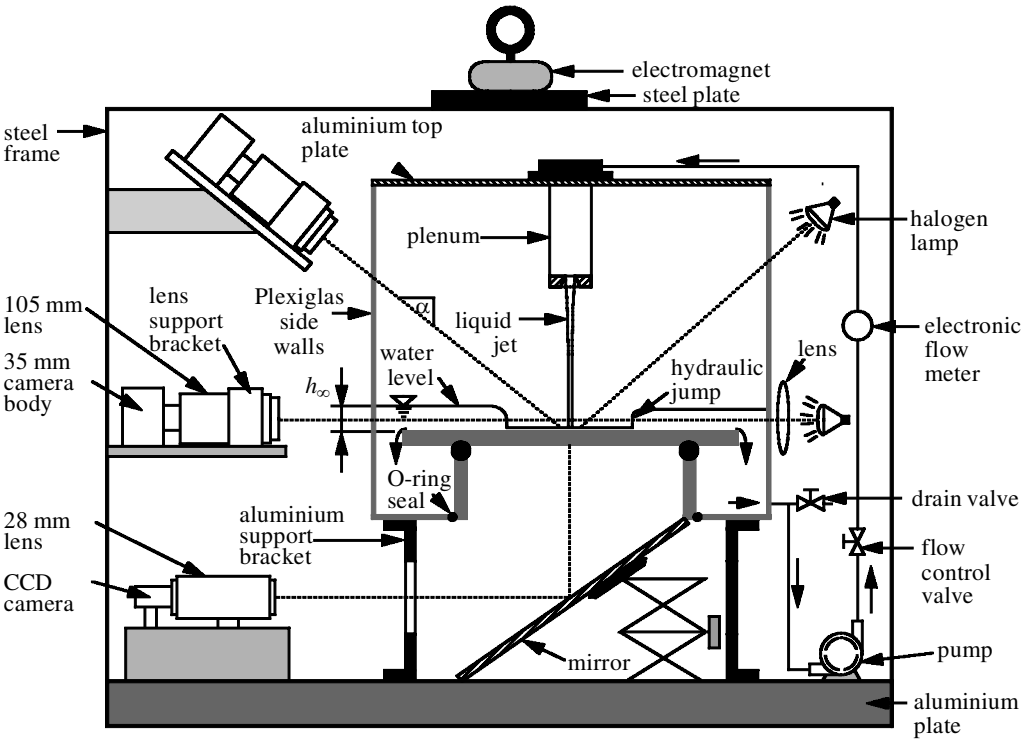

Figure 2. Schematic of flow loop mounted within the steel frame that is physically dropped to create low gravity.

under the tube allowed for observations of the underside of the jet. This view was a primary one to measure the CHJ radius. Additional viewing angles were along the plane to show the cross-sectional profile shape of the liquid film across the CHJ, and an angled top view for global features of the CHJ. The working fluid was water at room temperature in all the experiments.

To keep the design relatively simple, the primary means of data acquisition was photographic. A 35 mm Nikon F3 camera with MD-4 motor drive (operated at five frames per second) and with a 105 mm NIKKOR macro lens attached to it was used to record images at all three camera positions. Video images using a COHU CCD camera (30 images per second) were taken with a 28 mm NIKKOR macro lens to record the evolution of the CHJ in the transition to low gravity. All cameras and lenses were securely mounted to prevent damage due to the shock of the impact. Lighting was provided by halogen lamps (GE FHX, 13 W bulbs). The CHJ diameter was measured from video images of bottom views using a 'video caliper' (Video Caliper 306, Colourado Video Inc.) placed on the video image that was calibrated with a precision ruler (Schaedler Quinzel, Inc., USA) which was added to the image to calibrate (to ± 158 μm) the voltage output from the caliper. Side views were used to obtain the cross-sectional shape of the liquid film across the CHJ. The side-view images were fed into a MAC-based data acquisition system (Automatix Image Analysis Program) and an operator-selected grey scale was used to identify the various boundaries involved. A 19.05 mm diameter ball-bearing image converted the side-view pixel count to length with a precision of about ± 66 μm.

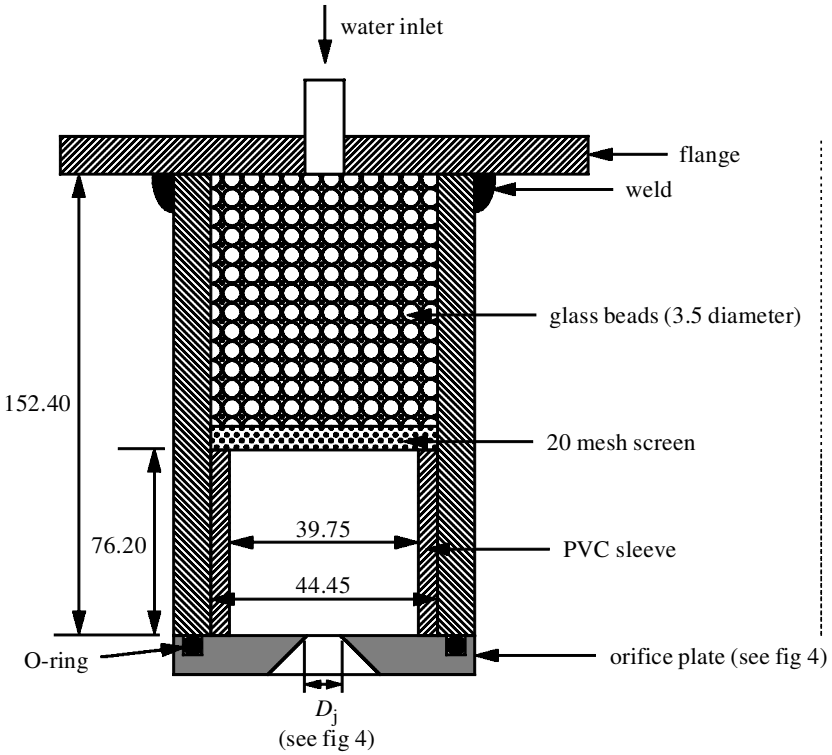

Figure 3. Plenum chamber design (dimensions in mm; not to scale).

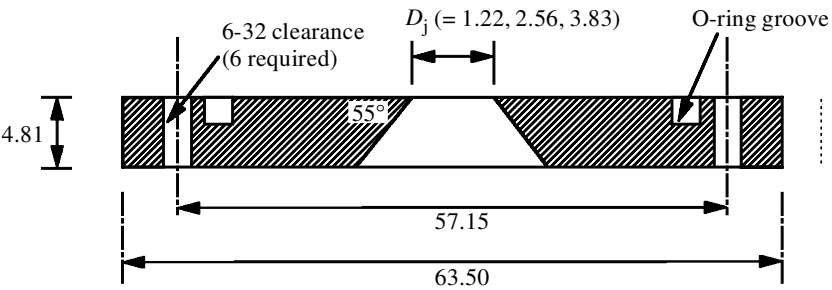

Figure 4. Design of sharp-edged orifice for producing laminar liquid jets (dimensions in mm; not to scale).

4. Discussion of results

(*a*) *Presentation of photographs and data*

In this section we present the main experimental results of the photographic documentation of the CHJ at low G, and quantitative measurements of the CHJ diameter. Further discussions about physical mechanisms for some of the observations are given in § 4 *b*.

Figure 5 is a photograph of a CHJ at $G = 1$ formed by impingement of a laminar water jet onto the target surface for the following conditions: $h_\infty = 4$ mm (i.e. the target plate was submerged to this depth); $D_j = 2.56$ mm; and a volumetric flow rate

Figure 5. Photograph of a laminar water jet striking the target surface ($D_j = 2.54$ mm; $Q = 9.57\ \mathrm{ml\ s^{-1}}$; $h_\infty = 4$ mm) at $G = 1$. The water jet is the rod-like structure. The CHJ is the dark outer ring bounding the upstream thin film.

Figure 6. Photograph of the water jet in figure 5 taken 200 ms after the period of low gravity begins. The transition zone upstream of the CHJ has considerably thinned indicating reduced curvature of the free surface. A 'hump' or large wave is visible immediately downstream.

(Q) of $9.57\ \mathrm{ml\ s^{-1}}$. The laminar liquid jet is the rod-like cylinder in the central portion of the photograph. The CHJ is the dark circular region that surrounds the bright thin film. The liquid film abruptly increases across the CHJ to match the downstream flow height which is a controlled variable. Waves are faintly visible in the upstream flow just before the CHJ. The downstream flow shows some mild disturbances but no clearly distinguished wave patterns.

When G is suddenly reduced, figures 6 and 7 show how the $G = 1$ CHJ of figure 5 reacts. Figure 6 was taken 200 ms after the period of free-fall. In the vicinity of the stagnation point the liquid continues to spread radially outward in a thin film, but at the start of the CHJ in $G \ll 1$ the curvature of the liquid–air interface across the jump decreases (or κ in figure 1 increases) and a 'hump' or large wave forms in the downstream flow followed by a a regular pattern of waves in the downstream flow.

Figure 7. Photograph of the water jet in figure 5 taken 400 ms into the $G \ll 1$ period.

These waves were commonly observed in all of the low-gravity conditions, and in the downstream flow at $G = 1$ for the smallest h_∞.

To better show the transition zone of the CHJ, subsurface photographs were taken by viewing from the side through the transparent wall of the containment tank. Figure 8 shows six photographs in series of the cross-section of the CHJ for $h_\infty =$ 4 mm spaced 200 ms apart. The photographs are aligned with the jet axis to show the changes in the CHJ during the transition to low G. Figure 8*a* shows the jump at $G = 1$ and figure 8*b*–*f* shows the flow situation at low G. As shown in figure 8*b*–*f*, the transition across the free surface to the downstream flow is more gradual at low G than $G = 1$ (figure 8*a*), which is consistent with the force balance of equation (1.5). The lengthening of the transition zone is also evident.

Figure 9 shows measurements of the shape of the free surface across the CHJ, digitized from the photographs in figure 8. Taking the CHJ to be the radial location where the film just starts to increase, the arrows mark the 'toe' of the CHJ. As is evident, the transition across the CHJ becomes more gradual when G is reduced.

A series of photographs to show the evolution of a CHJ at four different downstream heights for fixed flow rate is presented in figures 10 and 11. From figure 10 ($h_\infty = 2$ mm) the increase of the CHJ diameter is clear for $G \ll 1$ compared with $G = 1$, as shown by comparing parts (*a*) and (*c*) and parts (*d*) and (*g*) of figure 10. A large wave or 'hump' is visible at $t = 0.2$ s in figure 10*b*. Waves or ripples in the downstream flow are evident in figure 10*c*. For $h_\infty = 4$ mm (figure 10*d*–*g*) the CHJ diameter at $G = 1$ is smaller than for $h_\infty = 2$ mm at $G = 1$, which is consistent with equation (1.5) in that $D_\mathrm{h} \propto 1/H_\infty$. For $G \ll 1$ the CHJ diameter for $h_\infty = 5$ mm (figure 10*g*) is only slightly larger that for $h_\infty = 2$ mm (figure 10*c*). For $h_\infty = 10$ mm a CHJ did not form at $G = 1$ as shown in figure 11. On lowering G for the flow conditions shown in figure 11, a CHJ appeared.

Measurements of the evolution of CHJ diameter are shown in figures 12 and 13. The downstream height ($h_\infty = 4$ mm) and nozzle diameter were fixed and only the flow rate was changed. For the four flow rates shown the CHJ diameter was larger in $G \ll 1$ than in $G = 1$. For the conditions shown in these figures, a CHJ existed at $G = 1$. This effect is also seen in figure 9. For all such cases, a transient period

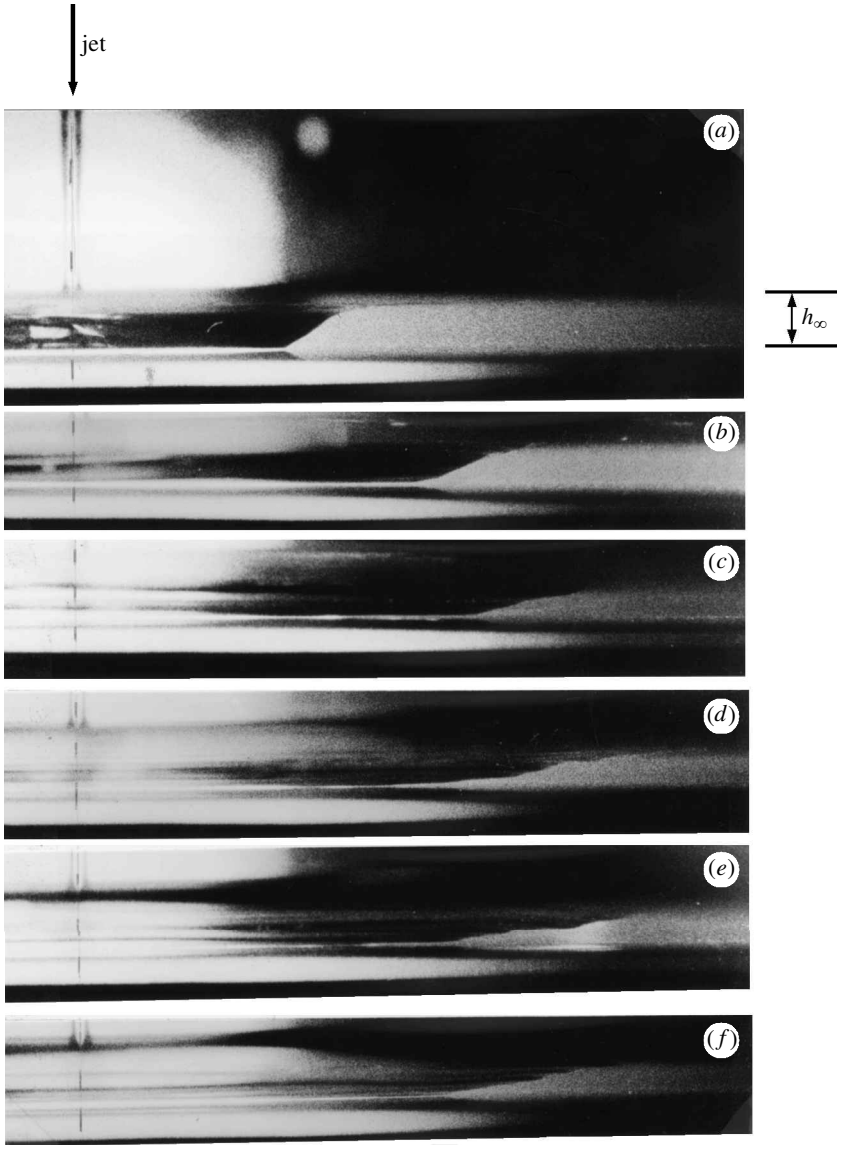

Figure 8. Side-view photographs of a water jet showing a cross-section of the liquid film across the CHJ for $h_\infty = 4$ mm and $Q = 6.32$ ml s^{-1} and $D_j = 1.22$ mm: (*a*) $G = 1$; (*b*)–(*f*) $G \ll 1$. The time between each photograph is 200 ms. The dashed line shows the position of the water jet.

of about 200 ms was sufficient to establish steady flow conditions in $G \ll 1$ after the sudden change in G. Thereafter, the CHJ diameter was constant in $G \ll 1$ as shown in figures 12 and 13.

The increase of the CHJ diameter at $G \ll 1$ relative to $G = 1$ is clearly illustrated by the three bottom-view photographs shown in figure 14. The dark circular zone in the centre of the photographs is the nozzle exit viewed through the underside of the transparent target plate. In these bottom-view photographs the $G \ll 1$ CHJ

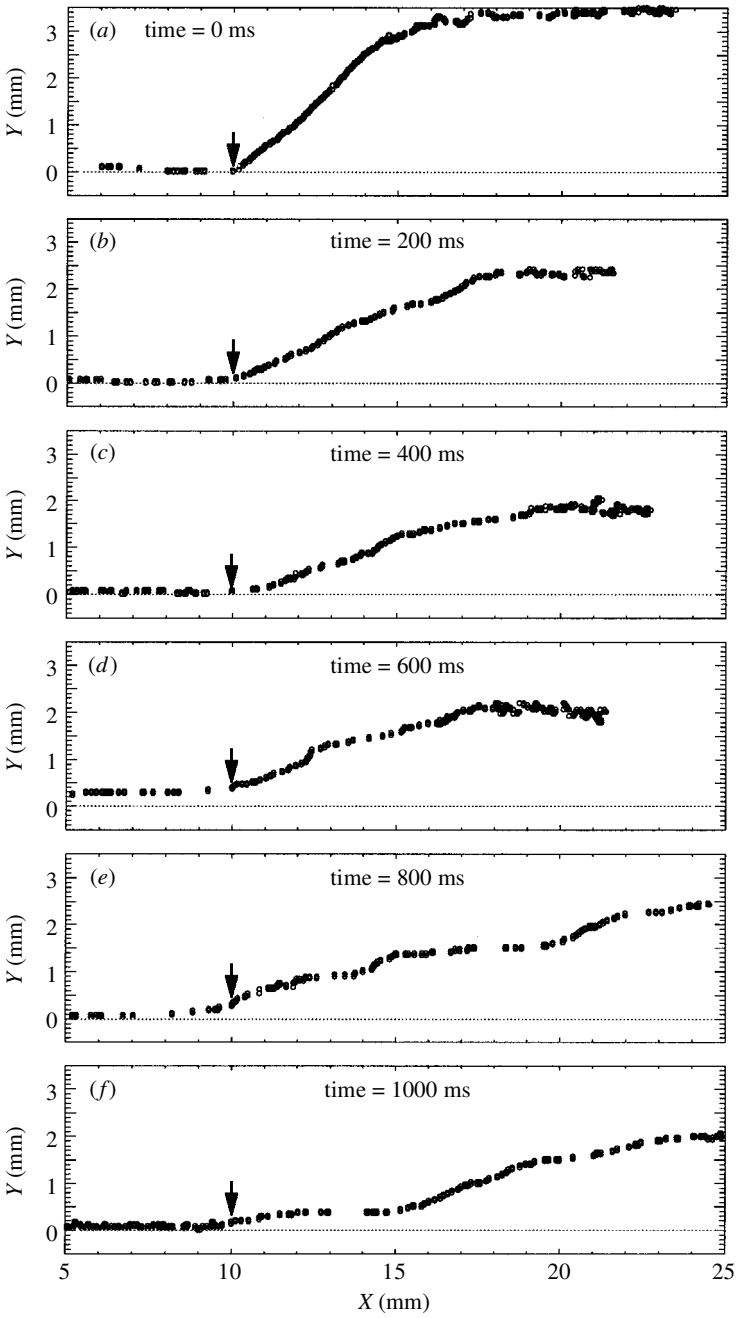

Figure 9. Measurements of the profile shape across the CHJ digitized from the photographs of figure 8. The figures are lined up with the CHJ, indicated by the arrow in each figure.

boundary is revealed at $t = 0.4$ s as the central circular zone of relatively uniform scattered light. The pattern of circular waves downstream of the CHJ is also visible in figure 14 at $t = 0.4$ s.

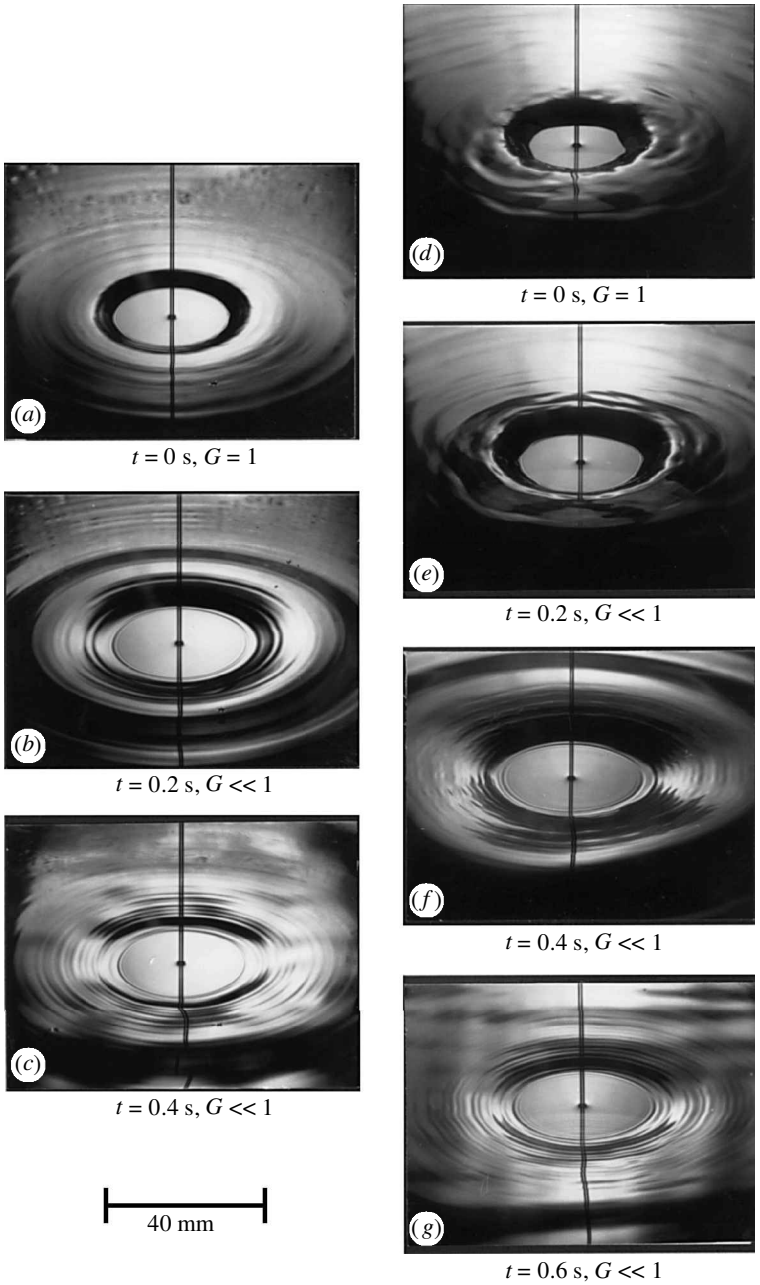

Figure 10. Photographic series of evolution of a CHJ during the transition from $G = 1$ to $G \ll 1$ in time-intervals of 200 ms with $Q = 6.32$ ml s^{-1} and $D_j = 1.22$ mm: (a)–(c) $h_\infty = 2$ mm; (d)–(g) $h_\infty = 4$ mm. During the transition the flow downstream of the CHJ thins indicating reduced curvature of the free surface and a large wave or 'hump' is visible $(b), (f)$, which propagates out of the field of view and leaves behind a series of concentric waves or ripples in the downstream flow.

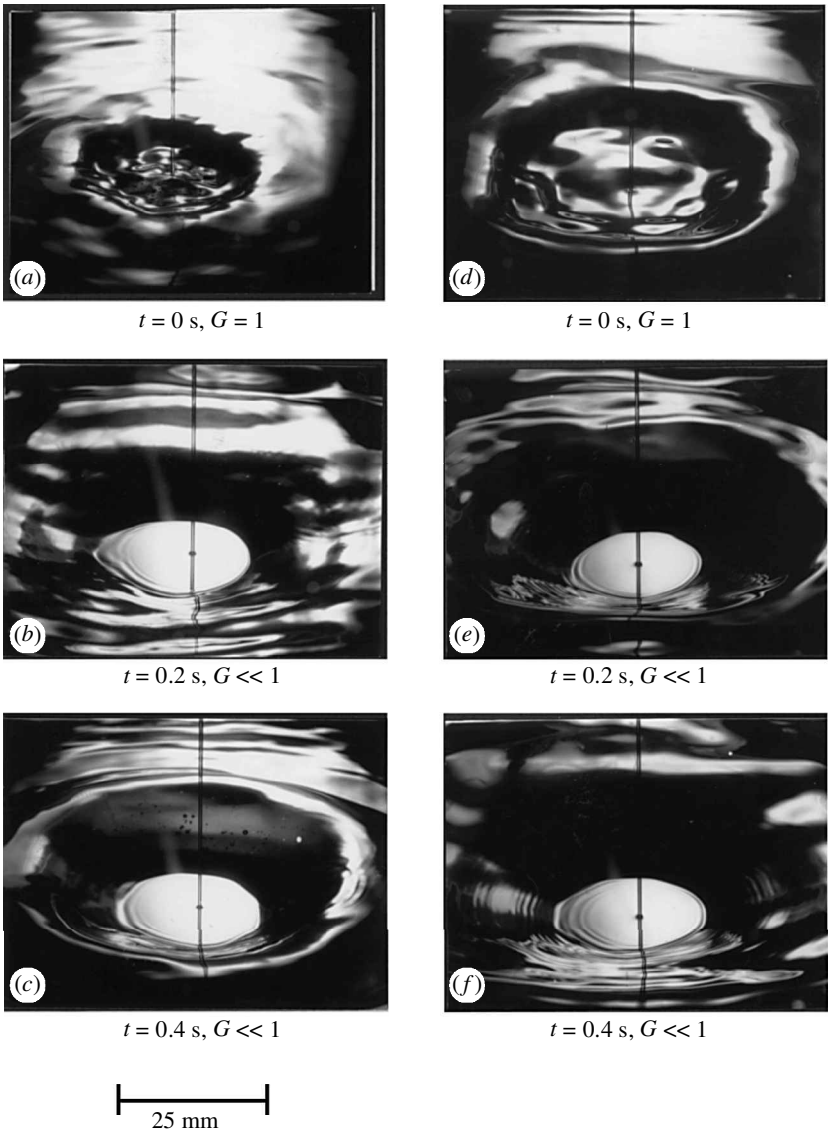

Figure 11. Photographic series showing development of a CHJ in $G \ll 1$ when a CHJ did not form at $G = 1$ because of the large downstream fluid height ($Q = 6.32$ ml s^{-1} and $D_j = 1.22$ mm): (a)–(c) $h_\infty = 10$ mm; (d)–(f) $h_\infty = 15$ mm.

For the largest values of h_∞ studied, 10 mm and 15 mm, a CHJ did not exist at $G = 1$ for $D_j = 1.22$ mm but was drawn out of the flow after the transition to $G \ll 1$ (see figure 11). Furthermore, the CHJ diameter did not attain a steady value during the period of the experiment. Figure 15 shows the evolution for the conditions of figure 11d–f. There was a brief period in which the liquid thinned considerably then gave way to the CHJ. After the CHJ appeared (figure 11e), the CHJ diameter never attained a steady-state value during the period of the experiment, as shown in figure 15.

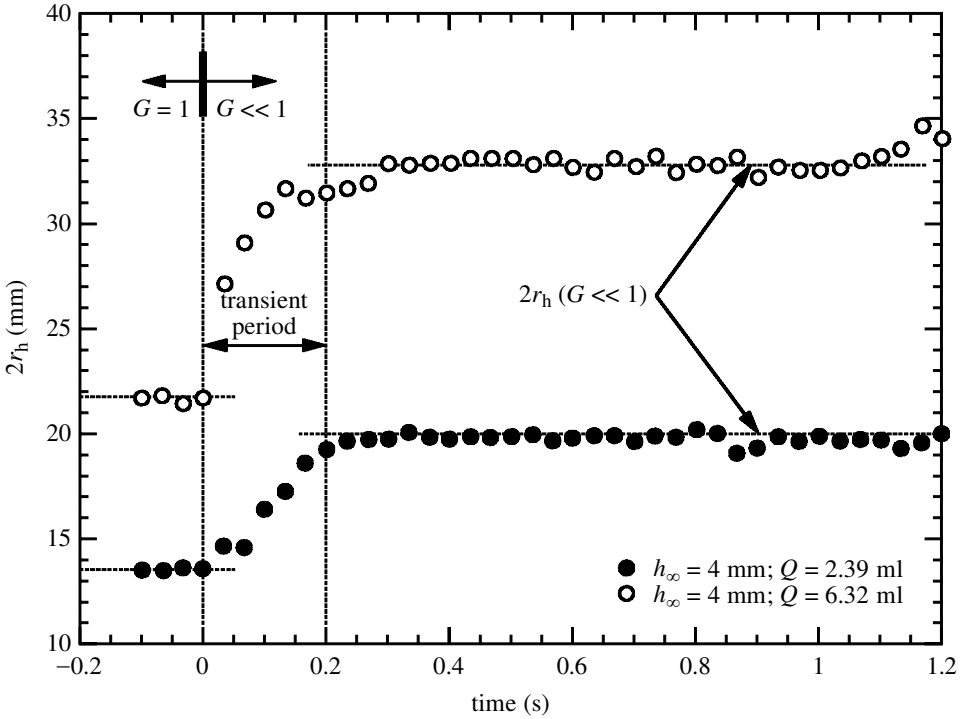

Figure 12. Evolution of the CHJ diameter ($2r_h$) showing the influence of flow rate (Q = 2.39 and 6.32 ml s^{-1}) for h_∞ = 4 mm and D_j = 1.22 mm. The transient period indicates the time over which the flow adjusts to the rapid change of G.

The variation of CHJ diameter with h_∞ for a flow rate of 6.32 ml s^{-1} is shown in figure 16. The lines shown in this figure are to suggest trends. For $h_\infty > 8$ mm at low gravity, the CHJ diameter was unsteady as shown in figure 15. For such conditions we took an average value of the CHJ diameter in the interval of 400–600 ms (see figure 15). As pointed out previously and quantitatively shown in figure 16, $D_{h,G=1} < D_{h,G\ll1}$. All of the $G = 1$ measurements (figures 12 and 13 show typical data) follow the trend that D_h decreases as H_∞ increases. However, at $G \ll 1$ the CHJ diameter appears to be independent of H_∞ as shown in figure 16. An explanation for these trends is offered in the next section.

How the CHJ evolves for the lowest flow rates examined, 2.39 ml s^{-1}, and the smallest downstream heights, 2 mm, is shown in figure 17. When h_∞ = 2 mm the CHJ at $G = 1$ is quite distinct as shown in figure 17*a*. However, surface waves are observed even at normal gravity for these conditions in figure 17. The transition to $G \ll 1$ (figure 17*b*, *c*) thins the transition zone and the CHJ increases slightly. Increasing h_∞ to 4 mm while maintaining Q at 2.39 ml s^{-1} moves the CHJ close to the stagnation point as shown in figure 17*d*, and considerable turbulence is observed in the downstream flow. However, in $G \ll 1$ the turbulent agitation in the downstream flow gives way to the regular pattern of circular waves as shown in figure 17*f*. Lowering gravity clearly effects the turbulent agitation in the transition and downstream flow: it eliminates it as shown in figure 17*d* ($G = 1$) and 17*f* ($G = 0.02$).

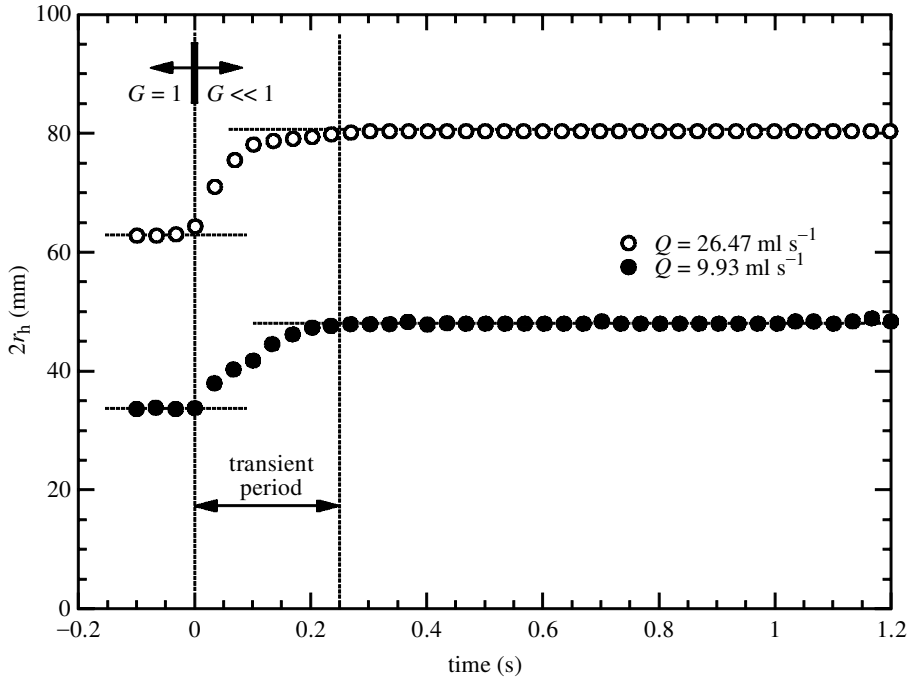

Figure 13. Evolution of the CHJ diameter ($2r_h$) showing the influence of flow rate ($Q = 9.93$ and 26.47 ml s^{-1}) for $h_\infty = 4$ mm and $D_j = 2.56$ mm. The transient period indicates the time over which the flow adjusts to the rapid change of G.

(*b*) *Explanation of results*

In this section we explain qualitatively the results of the previous subsection. These include the CHJ diameter, profile of the liquid shape across the jump, the length of the jump and downstream flow structure as G is reduced. Because a complete theory has not yet been developed for the CHJ that includes all of the effects observed, the discussion below is in many cases speculation about the mechanisms leading to the phenomena observed when G is reduced.

The influence of G is traced to the hydrostatic pressure (P_1) in the downstream film. This pressure balances the momentum of the upstream fluid and surface tension in the transition zone. Since $P_1 \propto g_0 G h_\infty$, reducing G or h_∞ will reduce the force that counterbalances fluid momentum. The result is a repositioning of the CHJ to a larger diameter where the velocity is lower because the velocity is inversely proportional to r_h. This effect is evident from the results presented in the previous subsection. Figure 14 shows the shift of the CHJ due to lowering G and figures 12 and 13 show quantitative measurements of the CHJ diameter increasing as G changes from $G = 1$ to $G = 0.02$.

Within the low-gravity environment of $G \approx 0.02$, D_h showed no definite trend with h_∞ as shown in figure 16 whereas at normal gravity the trend of equation (1.4) is followed. The disagreement of the low-gravity measurements with the trend of equation (1.4) can be explained by reconsidering the momentum balance which led to equation (1.2) but this time assuming that viscous effects dominate and gravity

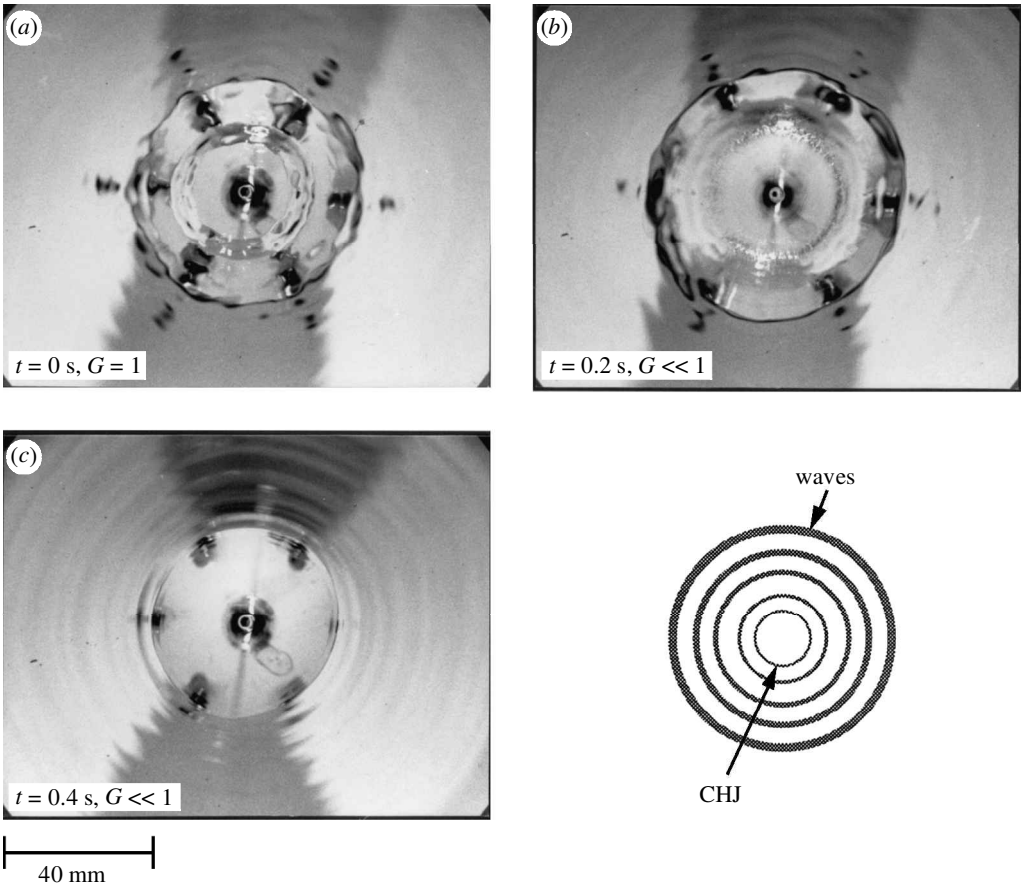

Figure 14. Series of three bottom-view photographs (viewed through the underside of the transparent target plate) of the water jet during the transition from $G = 1$ ($t = 0$ s) to $G \ll 1$ ($t = 0.2$ and 0.4 s). Ripples in the downstream flow are visible for $G \ll 1$. The increase of the CHJ diameter is apparent ($D_j = 2.56$ mm; $Q = 9.93$ ml s^{-1}; $h_\infty = 4$ mm).

is negligible. For this situation, we seek to determine how D_h scales with parameters when viscosity dominates over gravity in the CHJ.

The counterpart of equation (1.2), when drag at the plate in the transition zone of the CHJ balances fluid inertia, is obtained by a force balance around the control volume shown in figure 1 as

$$\left(\frac{r_j^2 U_j}{2r_h}\right)^2 \left(\frac{1}{h} - \frac{1}{h_\infty}\frac{r_h}{r_h + L_j}\right) \approx \frac{1}{2}\frac{L_j(2r_h + L_j)}{\rho r_h}\tau_w. \tag{4.1}$$

For the wall shear stress we use a rough scaling for a Newtonian fluid as a mean value between the velocity gradients at the wall upstream and downstream of the CHJ:

$$\tau_w = \mu\frac{\partial V_r}{\partial z} \approx \tfrac{1}{2}\mu\left(\left.\frac{\partial V_r}{\partial z}\right|_{r_h} + \left.\frac{\partial V_r}{\partial z}\right|_{r_h + L_j}\right) \approx \tfrac{1}{2}\mu\left(\frac{V_r}{h} + \frac{V_{r1}}{h_\infty}\right). \tag{4.2}$$

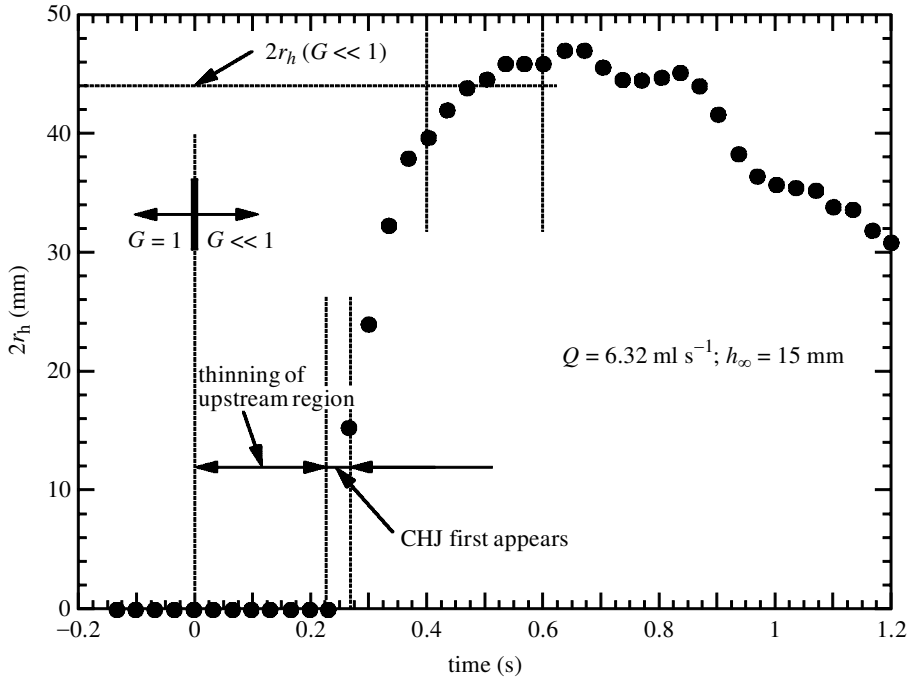

Figure 15. Evolution of the CHJ diameter ($2r_\mathrm{h}$) for conditions when a CHJ did not exist at normal gravity but was formed after reducing G ($h_\infty = 15$ mm; $Q = 6.32$ ml s^{-1}; and $D_\mathrm{j} = 1.22$ mm). The CHJ diameter is transient throughout the period of the experiment which is 1.2 s. A CHJ diameter for $G \ll 1$ was averaged over the measurements from 400 ms to 600 ms into the period of low gravity.

With mass conservation, the velocity components in the above equation are eliminated to give a relationship between the shear stress and parameters as

$$\tau_\mathrm{w} = \tfrac{1}{4}\mu \frac{U_\mathrm{j} r_\mathrm{j}^2}{r_\mathrm{h} H^2}\left(1 + \frac{h^2}{h_\infty^2}\frac{r_\mathrm{h}}{r_\mathrm{h} + L_\mathrm{j}}\right). \tag{4.3}$$

Substituting equation (4.3) into equation (4.1) and expressing the result in non-dimensional form gives

$$1 - \frac{H}{H_\infty}\frac{D_\mathrm{h}}{D_\mathrm{h} + 2\bar{L}_\mathrm{j}} = \frac{\bar{L}_\mathrm{j}(D_\mathrm{h} + \bar{L}_\mathrm{j})}{H Re_\mathrm{j}}\left(1 + \frac{H^2}{H_\infty^2}\frac{D_\mathrm{h}}{D_\mathrm{h} + 2\bar{L}_\mathrm{j}}\right). \tag{4.4}$$

It is reasonable to assume that $H/H_\infty \ll 1$, and if also $D_\mathrm{h} \gg \bar{L}_\mathrm{j}$, then equation (4.4) simplifies to

$$D_\mathrm{h} \approx H Re_\mathrm{j}/\bar{L}_\mathrm{j}. \tag{4.5}$$

To complete the scaling and arrive at the desired result we need to know how the upstream film thickness, H, depends on D_h. Middleman (1995) has shown that an energy balance in the upstream film in which the fluid kinetic energy is balanced by viscous dissipation when gravity is negligible yields

$$H = \frac{1}{2D_\mathrm{h}}\frac{1}{K(1 - (8/Re_\mathrm{j})\Phi(D_\mathrm{h}, H))}, \tag{4.6}$$

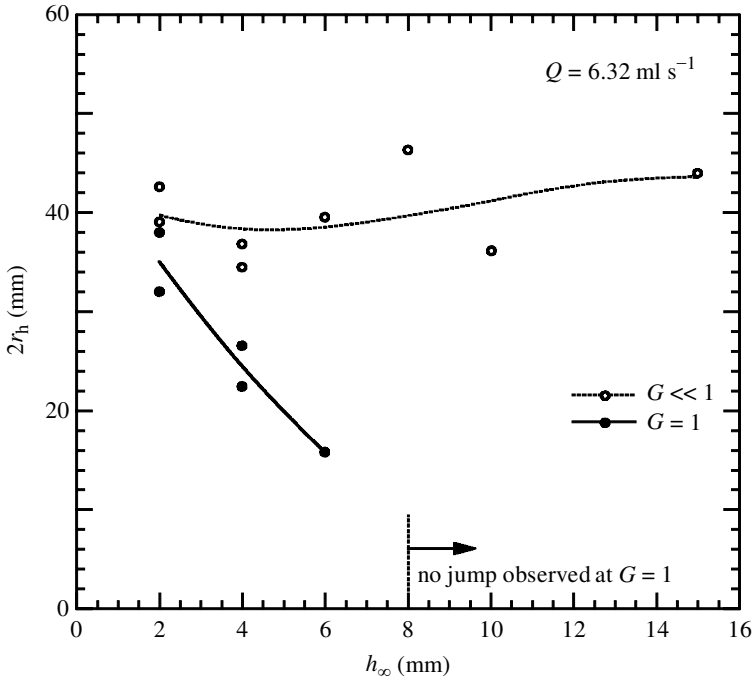

Figure 16. Variation of CHJ diameter with h_∞ for a given flow rate ($Q = 6.32\ \mathrm{ml\ s^{-1}}$ and $D_j = 1.22$ mm). The normal-gravity data follow the trend of equation (1.4) but the low-gravity measurements show no clear variation of the CHJ diameter with downstream fluid height.

where K is a factor (unity for a frictionless fluid) which depends on the form of the velocity profile in the upstream film and Φ is a dissipation function (zero for a frictionless fluid). Because Φ depends only on D_h and H, equation (4.6) implies a relationship for H as $H = f_1(Re_j, D_h, K)$ which, when combined with equation (4.5), implies an equation for D_h in terms of parameters as

$$D_h = f_2(Re_j, \bar{L}_j, K). \tag{4.7}$$

Equation (4.7) does not contain the downstream film height, H_∞. Thus, we see that if by reducing gravity viscous effects dominate, then the dependence of the CHJ diameter on H_∞ is removed. It is thus not surprising that D_h shows no dependence on h_∞ in low gravity, which is consistent with the data shown in figure 16.

The radius of curvature across the jump and downstream flow pattern are also influenced by G. The effect is again traced to the hydrostatic pressure in the downstream film. Concerning the radius of curvature, surface tension exerts a force which presses on the free liquid surface and the radius of curvature increases to balance the lower hydrostatic pressure brought about by reducing G. Concurrently, there is a more gradual transition from the upstream to the downstream flow, as seen in the side-view photographs in figure 8 and the digitized images in figure 9. Along with the increase in curvature across the CHJ and a more gradual transition to the downstream flow is a lengthening of the transition scale, L_j, in figure 1. This is evident by comparing figures 5 and 7 for $G = 1$ (figure 5) and $G = 0.02$ (figure 7). The increase of L_j brought about by decreasing G is consistent with equation (1.6), which was developed for planar jumps.

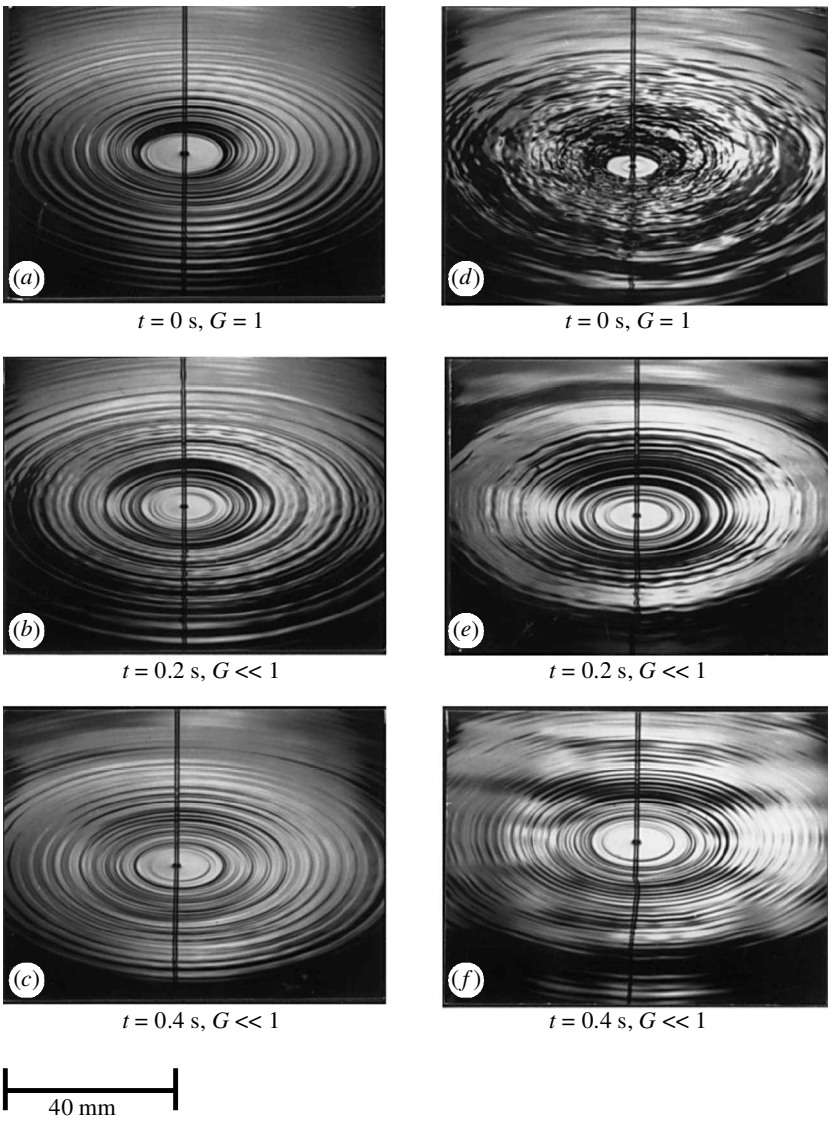

Figure 17. Photographs showing the development of the CHJ for the lowest flow rate examined, $Q = 2.39$ ml s^{-1}. For $h_\infty = 2$ mm (a)–(c) circular waves are visible in the downstream flow at normal gravity (a), showing that these waves are not unique to the low-gravity environment. For $h_\infty = 4$ mm (d)–(f) the CHJ diameter has moved very close to the jet and the downstream flow shows considerable agitation (d). When gravity is reduced $((d), (e))$, the downstream disturbances cease and give way to the regular pattern of circular waves shown in (f) ($D_j = 1.22$ mm; $Q = 2.39$ ml s^{-1}).

For all of the flow conditions at low gravity, waves in the downstream flow were observed at low gravity as shown in figures 7, 10c, f, 14 and 17. However, only for the smallest downstream depth, 2 mm, were they seen at normal gravity, as shown in figure 17a. Several mechanisms could promote formation of these waves. These include sudden reduction of the hydrostatic pressure brought about by dropping the

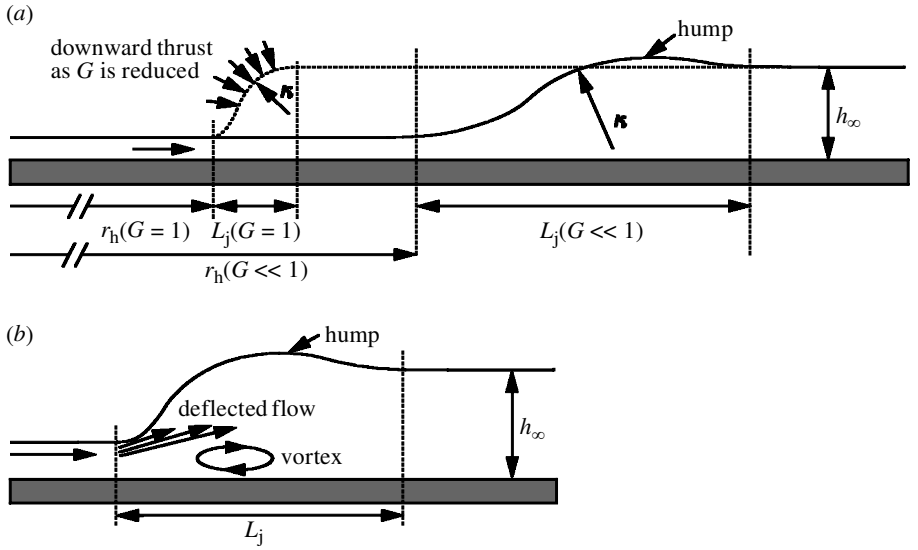

Figure 18. Schematic illustration of flow situations in the transition zone that could create waves in the downstream flow: (*a*) with rapid reduction of G surface tension pulls downward on the surface which increases the radius of curvature and increases the transition length; (*b*) flow past a wall vortex.

package with the result described above that the force due to surface tension at the free surface exerts a downward thrust across the transition zone, or separation and recirculation in the downstream film causing the oncoming flow to be deflected away from the target plate. There are several mechanisms which can create waves in the flow downstream of a CHJ. These include surface tension and formation of a vortex in the transition zone.

When G is suddenly reduced, surface tension will pull downward on the free surface and create ripples that propagate outward. Figure 18*a* is a schematic illustration of how this might be viewed. The close-up photographs of figures 5–7 show development of such a wave at the CHJ boundary. The hump just downstream of the CHJ in figure 6, 400 ms after low gravity begins, is the first evidence of it and figures 7, 10*b*, *e* and 14 show additional photographs. Figure 10*b*, *e* also shows a single large wave as it is just moving beyond the CHJ boundary.

A vortex which forms in the transition zone can deflect the flow away from the wall. Figure 18*b* illustrates this situation schematically. The effect of varying h_∞ on vortex formation and the consequences it has on the transition flow structure for normal-gravity CHJs have been discussed by Liu & Lienhard (1993*b*). At normal gravity, aspects such as flow reversal, surface rollers and separated eddies are observed to form if the hydrostatic pressure is considered to increase when h_∞ is increased. Within low G, the hydrostatic pressure in the downstream flow is already small so that the flow structure in the transition should be similar to the smooth-jump low-h_∞ cases discussed previously (Liu & Lienhard 1993*b*). In fact, all of the low-gravity conditions examined here showed a smooth transition across the CHJ.

Associated with formation of waves in the flow downstream of a CHJ at low gravity are the wave speed and wavelength. Inviscid deep-water theory is a useful perspective from which to understand the mechanisms which determine these quantities.

Waves for which surface tension controls propagation (i.e. 'ripples') have a smaller wavelength than 'gravity' waves from the inviscid theory (Milne-Thompson 1979). In low gravity, if surface tension dominates, we would then expect that $\lambda_{G\ll 1} < \lambda_{G=1}$. The evidence for this trend in our experiments is circumstantial because we could not measure the wavelength with sufficient accuracy. However, we see from figure 8*a* that the free surface is not as wavy at $G = 1$ as at $G \ll 1$, as also shown in figures 7 and 8*d*, *e*. From this we conclude that wave propagation in the downstream flow at low gravity is most probably controlled by surface tension.

For large downstream fluid film thicknesses, the response time of the CHJ to the reduction in gravity was longer than the experimental run time of 1.2 s. Figure 15 shows an example of the transient response of the CHJ diameter for $h_\infty = 15$ mm. The reason for the long adjustment time of the CHJ for the largest h_∞ examined may be traced to the characteristic response time of the fluid to a sudden disturbance. This time is of the order of (δ^2/ν), where δ is a characteristic fluid length-scale. Though a value for δ is open to question, if we assume that h_∞ is a reasonable characteristic length, then increasing the downstream fluid height by a factor of two would quadruple the response time. The largest heights examined showed a transient process that was longer than the experimental time (e.g. figure 15), in contrast to the smaller values of h_∞ in which the CHJ adjusted to the sudden change in G over times which were shorter than the experimental time (e.g. figures 12 and 13).

(*c*) *Comparison of measured CHJ diameter with theory*

The availability of theories for the CHJ motivated us to compare our measurements for steady-state flow conditions with predictions from one of them. The most elementary analysis of a CHJ neglects viscosity, as noted in § 1. Equations (1.2)–(1.4) result from making this assumption. The next level of complexity is to include viscous effects. Watson (1964) was one of the first to do this. A boundary layer model predicts the upstream velocity profile which was found to be self-similar at some radial distance away from the stagnation point. This theory has the essential features of more advanced treatments (see, for example, Bowles & Smith 1992; Higuera 1994) and is applied to the present data.

Watson (1964) considered two situations: a fully developed boundary layer ($r > r_0$ in figure 1) and a developing profile for the flow in the upstream thin film, $r < r_0$ (figure 1). The anslysis assumes that $h_\infty^2 \gg h^2$, it ignores viscous effects in the downstream flow and a similarity solution is derived to the boundary layer equations for the flow in the thin film upstream of the CHJ. Middleman (1995) expressed the solution in terms of the following non-dimensional variables:

$$Re_\mathrm{j} \equiv \frac{4Q}{\pi D_\mathrm{j}\nu}, \quad d_\mathrm{h} \equiv D_\mathrm{h} Re_\mathrm{j}^{-1/3}, \quad \bar{H} \equiv H_\infty Re_\mathrm{j}^{-1/3}, \quad Y \equiv \frac{d_\mathrm{h}\bar{H}}{Fr_\mathrm{j}} + \frac{1}{2d_\mathrm{h}\bar{H}}.$$

In terms of Y and d_h the results are as follows:

$$Y = \frac{0.26}{d_\mathrm{h}^3 + 0.287} \tag{4.8}$$

when $r < r_0$ ('developing' flow) and

$$Y = 1 - 1.02 d_\mathrm{h}^{3/2} \tag{4.9}$$

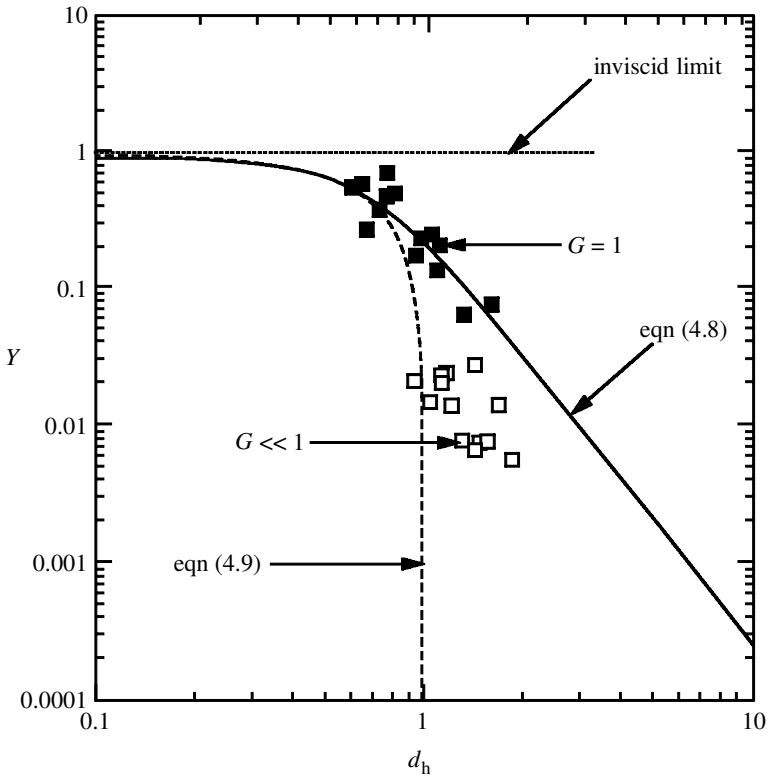

Figure 19. Comparison of the CHJ measurements with the theory of Watson (1964) cast in the variables of Middleman (1995) (equations (4.8) and (4.9)).

when $r > r_0$ ('fully developed' flow). The inviscid limit is $d_h \to 0$ and $Y = 1$ in equation (4.9) (remembering that the approximation $h_\infty^2 \gg h^2$ was applied). Y and d_h are known from the experimental results: $2r_h$ (the CHJ diameter) is measured; and h_∞ and Q are control parameters ($U_j = Q/[\frac{1}{4}\pi D_j^2]$) of the experiment. For the water kinematic viscosity at 300 K, $\nu \approx 8.95 \times 10^{-7}\,\mathrm{m^2\,s^{-1}}$ (Keenan *et al.* 1969). An average G of 0.02 is used over the free-fall distance.

Figure 19 shows the variation of Y with d_h. The inviscid limit does not predict our measurements. The measurements are bounded by the developing flow (equation (4.8)) and fully developed flow limit (equation (4.9)) for both the normal- and low-gravity data. The normal-gravity measurements are reasonably well predicted by assuming the flow to be developing in the upstream film, in that the boundary layer (figure 1) has not yet reached the free surface. On the other hand, the low-gravity data shown in figure 19 are closer to the fully developed flow prediction of equation (4.9), though still not quantitatively predicted by that limit. This general result is consistent with the increased upstream flow length (i.e. larger CHJ diameter) when gravity is lowered. With the larger flow length at low gravity, the flow in the upstream thin film has a chance to become more developed. The fact that the low-gravity data are bounded by the developing and fully developed limits shows that the analysis which leads to equations (4.8) and (4.9) is a reasonable model for the conditions of our experiments.

The agreement shown in figure 19 could be viewed as unusually good given what is not included in the analysis: the CHJ is treated as a discontinuity in the analysis, whereas in reality the transition to the downstream flow occurs over a finite length which is more extended in low gravity; there are waves in the downstream flow; the flow downstream of the CHJ may separate and form a circulation eddy; and vorticity generation at the CHJ is not included. Some of these aspects have been considered individually in prior studies as outlined in § 2. Including all of them at once is a challenge for future work. Finally, if G were identically zero, analyses by Thomas *et al*. (1990) and Rahman *et al*. (1990) as well as equation (1.4) predict that a CHJ would not form. While we do not achieve this limit in our study ($G \approx 0.02$ as noted previously), the larger CHJ diameter at low gravity compared with normal gravity is consistent with these predictions.

5. Summary

The results are summarized as follows.

(1) A steady CHJ can be established in low gravity ($G \neq 0$) and the CHJ diameter at low gravity is larger than at normal gravity for the same jet conditions.

(2) The response time of the CHJ to a sudden transition in gravity is less than 200 ms when a jump exists at normal gravity for the flow conditions examined.

(3) The curvature of the free surface across the CHJ decreases when gravity is reduced and the transition to the downstream flow is more gradual than at normal gravity.

(4) Suddenly reducing gravity produces a large wave or hump just downstream of the transition zone across the CHJ which propagates into the downstream film and concentric waves form in the downstream flow at low gravity.

(5) The variation of the CHJ diameter with downstream film thickness at normal gravity qualitatively (but not quantitatively) follows the trend of the inviscid theory at normal gravity, but the trend is not followed for the low-gravity measurements.

(6) Measured CHJ diameters are bounded by the two limits of fully developed flow and developing flow, with the normal-gravity measurements reasonably well predicted by assuming developing flow in the upstream film and the low-gravity measurements falling between the two limits.

We thank Jun-Eu Tang and Hanwook J. Kim of Cornell for helping with the experiments and Jack Salzman (NASA) for drawing the authors' attention to Labus (1976). This study was supported in part by NASA under grant NAG 3-1627 (Bradley Carpenter, Program Director and David Chao, Project Monitor) and by the Semiconductor Research Corporation (task 96-004).

Nomenclature

Bo	Bond number ($\equiv \rho G g_0 h_\infty r_\mathrm{j}/2\sigma$)
D_j	orifice diameter, figure 1

D_h $\equiv r_h/r_j$
d_h $\equiv D_h Re_j^{-1/3}$
Fr Froude number based on average liquid film velocity just before CHJ ($\equiv U^2/Gg_0h$)
Fr_j Froude number based on average velocity of impinging jet ($\equiv U_j^2/Gg_0h_\infty$)
g local gravitational acceleration within free-fall package
g_0 Earth's normal gravity ($= 9.8\ \mathrm{m\ s^{-2}}$)
G $\equiv g/g_0$
h_∞ liquid film thickness immediately downstream of the CHJ (see figure 1)
h liquid film thickness immediately upstream of the CHJ (see figure 1)
H $\equiv h/r_j$
H_∞ $\equiv h_\infty/r_j$
$\bar{H}$ $\equiv H_\infty Re_j^{-1/3}$
L_j length of jump (figure 1)
$\bar{L}_j$ L_j/r_j
P fluid pressure in liquid film immediately upstream of the CHJ
P_1 fluid pressure in liquid film immediately downstream of the CHJ
Q volumetric flow rate
Re_j Reynolds number ($\equiv 2Q/\pi r_j\nu$)
r_j radius of orifice ($= D_j/2$)
r_h radius of the CHJ
U average velocity of liquid film immediately upstream of the CHJ
U_j average velocity of jet at orifice
V_{r1} local velocity within liquid film immediately downstream of the CHJ (see figure 1)
V_r local velocity within liquid film immediately upstream of the CHJ (see figure 1)
Y $\equiv (d_h\bar{H}/Fr_j) + (1/2d_h\bar{H})$
z coordinate normal to the target plate
κ radius of curvature of the free surface in the transition zone across the CHJ (see figure 1)
$\bar{\kappa}$ $\equiv \kappa/r_j$
λ length of waves in the downstream flow
ρ liquid density
σ surface tension
ν liquid viscosity

References

Allen, T. & Ditsworth, R. L. 1972 *Fluid mechanics*, p. 291. New York: McGraw-Hill.

Avedisian, C. T., Yang, J. C & Wang, C. H. 1988 On low gravity droplet combustion. *Proc. R. Soc. Lond.* A **420**, 183–200.

Bowles, R. I. & Smith, F. T. 1992 The standing hydraulic jump: theory, computations and comparisons with experiments. *J. Fluid Mech.* **242**, 145–168.

Bouhadef, M. 1978 Etalement en couche mince d'un jet liquide cylindrique vertical sur un plan horizontal. *Z. Angew. Math. Phys.* **29**, 157–167.

Chaudhury, Z. H. 1964 Heat transfer in a radial liquid jet. *J. Fluid Mech.* **20**, 501–511.

Craik, A. D. D., Latham, R. C., Fawkes, M. J. & Gribbon, P. W. F. 1981 *J. Fluid Mech.* **112**, 347–362.

Errico, M. 1986 A study of the interaction of liquid jets with solid surfaces. PhD thesis, University of California, San Diego.

Hager, W. H. 1993 Classical hydraulic jump: free surface profile. *Can. Jl Chem. Engng* **20**, 536–539.

Higuera, F. J. 1994 The hydraulic jump in a viscous laminar flow. *J. Fluid Mech.* **274**, 69.

Hornung, H. G., Willert, C. & Turner, S. 1995 The flow field downstream of a hydraulic jump. *J. Fluid Mech.* **287**, 299–316.

Keenan, J. H., Keys, F. G., Hill, P. G. & Moore, J. G. 1969 *Steam tables*, p. 114. Wiley.

Labus, T. L. 1976 Liquid jet impingement normal to a disk in zero gravity. PhD thesis, University of Toledo.

Liu, X. & Lienhard, J. H. 1993*a* Extremely high heat fluxes beneath impinging liquid jets. *J. Heat Transfer* **115**, 472–476.

Liu, X. & Lienhard, J. H. 1993*b* The hydraulic jump in circular jet impingement and in other thin liquid films. *Exp. Fluids* **15**, 108–116.

Middleman, S. 1995 *Modeling axisymmetric flows*, ch. 5. Academic.

Milne-Thompson, L. M. 1979 *Theoretical hydrodynamics*, 5th edn, p. 448. London: Macmillan.

Nirapathdongporn, S. 1968 Circular hydraulic jump. MEng thesis, Asian Institute of Technology, Bangkok, Thailand.

Rahman, M. M., Faghri, A. & Hankey, W. L. 1990 New methodology for the computation of heat transfer in free surface flows using a permeable wall. *Numer. Heat Transfer* B **18**, 23–41.

Streeter, V. L., Wylie, E. B. & Bedford, K. W. 1998 *Fluid mechanics*, 9th edn, pp. 372, 610–612. New York: McGraw-Hill.

Tani, I. 1949 Water jump in the boundary layer. *J. Phys. Soc. Jap.* **4**, 212–215.

Thomas, S., Hankey, W. L., Faghri, A. & Swanson, T. 1990 One-dimensional analysis of the hydrodynamic and thermal characteristics of thin film flows including the hydraulic jump and rotation. *J. Heat Transfer* **112**, 728–735.

Watson, E. J. 1964 The radial spread of a liquid jet over a horizontal plane. *J. Fluid Mech.* **20**, 481–499.

Womac, D. J., Ramadhyani, S. & Incropera, F. P. 1993 Correlating equations for impingement cooling of small heat sources with single circular liquid jets. *J. Heat Transfer* **115**, 106–115.